IEEE Access
Multidisciplinary ⋮ Rapid Review ⋮ Open Access Journal

Received October 27, 2021, accepted November 17, 2021, date of publication November 19, 2021,
date of current version November 30, 2021.

Digital Object Identifier 10.1109/ACCESS.2021.3129736

A Travelling Wave-Based Fault Location Strategy Using the Concepts of Metric Dimension and Vertex Covers in a Graph

ELIZABETH C. M. MARITZ[1], JACQUES M. MARITZ[2], AND MOSLEM SALEHI[3]
[1]Department of Mathematics and Applied Mathematics, University of the Free State, Bloemfontein 9301, South Africa
[2]Engineering Sciences, University of the Free State, Bloemfontein 9301, South Africa
[3]Department of Electrical Engineering, Faculty of Khorramabad, Lorestan Branch, Technical and Vocational University (TVU), Tehran 1435661137, Iran

Corresponding author: Elizabeth C. M. Maritz (maritzecm@ufs.ac.za)

ABSTRACT This paper presents a novel travelling wave-based placement strategy and fault detection scheme to locate faults on complex power grids. A fault occurring on a power grid results in travelling waves propagating from the fault location towards detectors. In this paper, the power grid is transformed to a simple, weighted, undirected graph and the shortest path information is leveraged using two well-known graph invariants to place detectors and detect and locate faults accurately. An offline algorithm is presented to determine the number and position of detectors, while an online algorithm is proposed for locating the fault. The proposed fault detection algorithm is benchmarked using the IEEE 30-bus distribution system.

INDEX TERMS Metric dimension, locating set, resolving set, vertex cover, travelling wave fault location and grid protection.

I. INTRODUCTION

Managing the supply and integrity of energy depends on the ability to understand, protect and control a complex power system in an optimized and real-time manner [1]. The ability to respond to faults, and the restoration process following thereafter, relies on a wide area situational awareness of the grid and the fault status of the electrical network [2]. Hardware protocols with short delays and fast sampling allow for synchronized grid information that can be leveraged for the purposes of low latency digital resource optimization, grid protection and fast demand response [3]–[5], see Fig. 1.

To support the notion of a self-healing smart grids and microgrids, especially those with complex grid topologies, the concept of fault location via the detection of travelling waves is receiving attention spread across numerous fundamental fields of science and engineering, with particular application in graph theory [6], [7]. The concept of travelling wave fault location (TWFL) is firmly based on the physics model that governs the propagation of the wideband disturbance wave and ability to detect the wave in a synchronized and accurate manner using TWFL detectors [8].

The associate editor coordinating the review of this manuscript and approving it for publication was Bin Zhou.

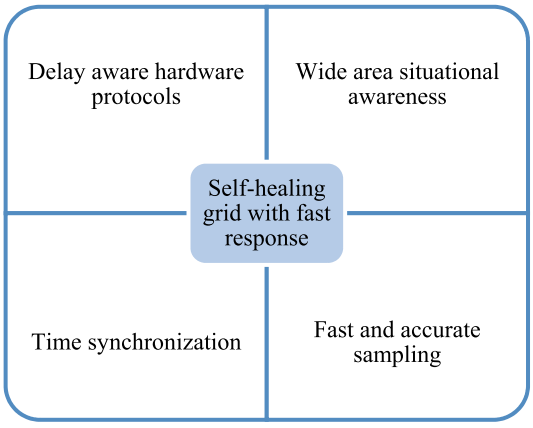

FIGURE 1. Interplay of the time and frequency domain for grid protection hardware to ensure fast response to faults and self-healing.

TWFL is driven by wave arrival times and prior knowledge of the network topology, ultimately providing an elegant detection method for fault location. TWFL optimizes both the restoration time needed following fault detection (and location) and the network response to protect against damage associated with valuable electrical infrastructure, wild fires and loss of life [9]. Grid failure is considered to be a global problem, but is intensified for countries with

poorly maintained and aging infrastructure. TWFL detection schemes are sensitive to the number of detectors, since fault waves are considered to be fast transients and require costly detectors with high frequency sampling properties, hence the number of detectors required must always be minimized [9], [10].

TWFL detection schemes exist for overhead transmission lines, hybrid transmission lines and wide area distribution networks [11]. However, the emphasis is shifting to smaller power systems (e.g. university campus microgrids and low voltage networks) and the TWFL opportunities that these scenarios offer. TWFL techniques associated with transmission lines (whether hybrid or not) have the added benefit of large distances supporting the delay and detectability between the successive reception of disturbance waves. The value of these techniques decreases with compact networks that consist of relatively short paths between the electrical buses in the network. With the development of synchrophasors to establish a true real-time representation of a power grid comes the opportunity of accurate and time-aligned TWFL measurement [12]. The reader is referred to [13] for a detailed comparison of different detection techniques and the influence of sampling rate and time synchronicity on such alternative methods. These include impedance-based techniques, requiring voltage, current and the impedance sequence to estimate the location of the fault [13], [14]. In [15], hybrid classifiers were investigated for fault location in distribution networks. S-transform-based feed forward neural networks were investigated in [16] for distribution grid networks, which are able to detect faults independent of the physical limitations associated with traditional TWFL detection schemes. Furthermore, [17] and [18] investigated the applicability of wavelet transforms (representation of transient in time and frequency) towards support vector machine and extreme learning applications in distribution grids. TWFL detection schemes work well for fault location associated with transmission lines, due to full control of the physical effects influencing the accuracies of fault locations [9]. The traveling wave detection requirements (both hardware and software) become more stringent for compact grid topologies, such as campuses and cities [19]. In these cases, the emphasis is placed on the data processing techniques associated with voltage and current measurements at key locations. Due to the short travelling times (microseconds) and wide band nature of the TW within the grid topology, detection instruments are typically utilizing high-frequency sampling and time synchronization capabilities with other instruments [9] and is tied to the concept of grid observability [20], [21].

This paper proposes an alternative travelling wave-based placement strategy and fault detection scheme for fast and accurate fault detection. The objectives of this study were to develop a placement criteria for a minimum amount of detectors, and to demonstrate an online algorithm for locating faults within the grid. For the first objective, two well-known graph invariants, the metric dimension [22]–[25] and vertex cover [24], [26], are used as part of an offline algorithm to determine the number and placement of detectors. Simulations were also conducted on a standard IEEE 30-bus to test the applicability and accuracy of the proposed method. The paper is structured as follows: Section II briefly summarizes the physics of TWFL detection. Section III explores the graph theory and the invariants used in the pre-processing offline algorithm to determine the number and placement of detectors in the grid. Section IV contains the fault location methodology based on the given detector placement. In Section V, simulations are carried out on the IEEE 30-bus, followed by a discussion in Section VI and the conclusion in Section VII.

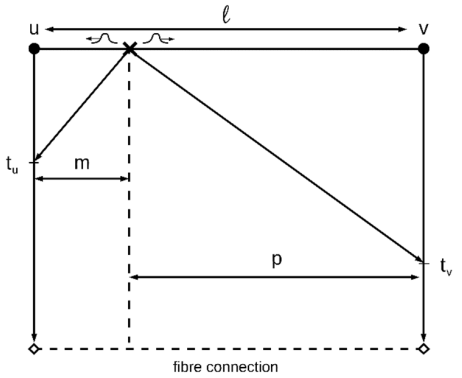

FIGURE 2. Fault occurrence (marked "X") between two buses generating a wideband travelling wave propagating towards TWFL detectors positioned at u and v. The distances travelled are denoted by m and p, and the detectors accurately measure the arrival times t_u and t_v of the primary and secondary fault disturbance waves.

II. PHYSICS OF TWFL

This section contains a brief summary of fault location via traveling waves. The reader is referred to [9] for a detailed overview of TWFL detection.

Consider an elementary power grid G having only 2 buses u and v with an edge connecting them. A fault occurring somewhere on this edge of G generates a travelling disturbance that is a wide frequency phenomenon and includes a plethora of physical effects that closely follow the characteristics of the particular electrical network that the graph represents [9], [10], [27], [28], [29]. If detectors are positioned at u and v and a fault occurs somewhere along the edge as illustrated in Fig. 2, travelling waves will propagate from the fault towards u and v by means of the shortest path possible.

In general, a fault occurring along any line will result in waves propagating through the grid toward the detectors. The primary waves reaching the detectors will clearly follow the shortest path between the fault and a detector, while reflected (refracted) waves reach the detectors through other paths in the grid. The methodology relies on using the primary travelling waves arriving at detectors u and v, and to extract their times of arrival t_u and t_v, respectively. In this particular instance as shown in Fig. 2, it is then possible to calculate the shortest distance m from the fault to detector u, using the following equation,

$$m = \frac{l_{uv} + (t_u - t_v)\, v}{2} \tag{1}$$

where l_{uv} is the cable length of line uv, and v is the speed along line uv. The fraction $x^{uv} = \frac{m}{l}$ of the total length of uv can be found from the equation

$$x^{uv} = \frac{T_{uv} + (t_u - t_v)}{2T_{uv}}, \tag{2}$$

where T_{uv} is the transmission time along line uv [30].

The example in Fig. 2 shows a double-ended detection method, but TWFL techniques can span single-ended, double-ended or wide area detection methods based on the number of detectors and the ability to detect the primary or reflected waves.

The accuracy of fault wave times of arrival and inherent errors associated with the fault location depends on several physical effects that are detector-based or governed by the electrical network. Latter-mentioned network effects include dispersion of travelling waves and the impact of branch incident waves [9]. Detector based effects include sampling rates and time detector synchronization errors [10].

Travelling fault waves within complex networks pose the challenge of dealing with the composition of primary (shortest path) waves and reflected waves. Both generations of waves are wideband in the frequency domain and complex by nature, but the reflected (or refracted) waves are attenuated versions of the primary wave [29].

TWFL schemes can utilize different levels of data associated with the primary waves and reflected waves, including primary wave arrival times, secondary wave arrival times, wave polarities and detection triggers from neighboring fiber linked detectors. For single ended detection, both primary and secondary wave time stamps are utilized. For double ended detection, the time stamps associated with the primary waves detected at both ends, are utilized [10].

III. OPTIMAL PLACEMENT OF DETECTORS

In this section, a brief introduction to graph theory and parameters involved in detector placement and fault location will be presented. A graph $G = \{V, E\}$ consists of nodes or vertices in a set $V(G)$, and possible connections or edges between them, denoted by $E(G)$. Only simple, undirected graphs are considered, meaning there are no loops (an edge from a vertex to itself) and there can be at most one edge $e = uv = vu$ between every two vertices u and v. Positive integers n and m represent the number of vertices and edges in a graph, respectively, and these are referred to as the *order* and *size* of G. If an edge connects two vertices u and v, they are said to be *adjacent*, and the graph G can be represented by its adjacency matrix A [26], which is an $n \times n$ matrix with entries

$$a_{ij} = \begin{cases} 1 & \text{if } v_i v_j \in E(G), \\ 0 & \text{otherwise.} \end{cases} \tag{3}$$

It is clear that if G is a simple graph, the main diagonal of A would consist of zeros, and if G is undirected, A would be a symmetric matrix. The *degree* of a vertex v, or $\deg(v)$, is the total number of edges that are incident with v, which can be found by adding the entries in the row corresponding to v.

The power grid is modelled using a graph where the vertices represent buses, with labeled edges denoting the cable length between them, and the notion of locating sets in graphs is applied as an attempt to resolve vertices, edges and, ultimately, any position within an edge accurately. One additional advantage of using graphs to model power grids is that the vulnerability of the grid can be evaluated by considering the *density* of G, which is the ratio of edges in the graph in relation to the maximum number of possible edges,

$$D = \frac{2|E(G)|}{|V(G)|(|V(G)| - 1)}. \tag{4}$$

The concept of distance plays a central role not only in the resolvability of vertices and edges in a graph, but also in constructing a model of a power grid. For the moment, only unweighted graphs are considered (edges are unlabeled), but in application the physical distance would also have to be represented in the model, and for this an edge $e = uv$ is labelled with a weight l_{uv}, where l_{uv} denotes the physical length of a cable connecting vertices u and v. Hereafter, such a graph shall be referred to as a *power grid graph,* where vertices u and v represent buses and an edge between them a physical cable of a certain length connecting them. For now, the distance between any two vertices u and v in an unweighted connected graph G is defined to be the number of edges in a shortest path from u to v, denoted by $d(u, v)$ [26].

Distance in graphs give rise to many parameters, of which we include the metric dimension in Section III(A), and a few others here, for the purposes of this paper. For more detail or terminology the reader is referred to [26].

The *eccentricity* of a vertex v is the maximum distance between v and all other vertices in the graph. The *diameter* d of a connected graph G is the maximum eccentricity, or the greatest distance between any two vertices in the graph, and by the same token the *radius* is the minimum eccentricity. All vertices of minimum eccentricity form the *center* of the graph, and all vertices of maximum eccentricity form the *periphery* of the graph.

A. METRIC DIMENSION

The metric dimension of a graph is essentially the smallest number of landmarks necessary to provide a set of unique coordinates to different sites, based on their distances to these landmarks [24], [25]. Slater fittingly referred to this set of landmarks as a *locating* set in [22] and originally proposed its usefulness in working with sonar and loran stations. The terminology of Harary and Melter [23] will be used throughout this paper.

Suppose k vertices in a graph are selected to form an ordered set $W = \{w_1, w_2, \ldots, w_k\}$, as seen in Fig. 3. For each vertex v in G, a code (in the form of a k-tuple) can be formed consisting of the distances from v towards each of the vertices $w_1, w_2, \ldots, w_k$ in W. This is called the *metric representation of v with respect to W* and is defined as

$$r(v \mid W) = (d(v, w_1), d(v, w_2), \ldots, d(v, w_k)) \tag{5}$$

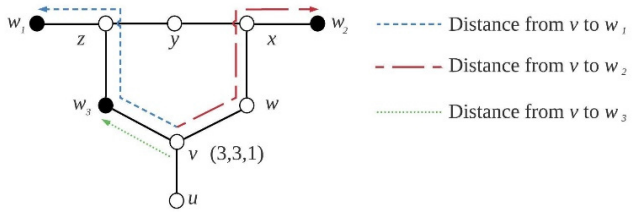

FIGURE 3. Example of a graph where three vertices (solid) are selected to form a set $W = \{w_1, w_2, w_3\}$. The vertex v with its metric representation with respect to W is shown, namely $r(v \mid W) = (3, 3, 1)$ and the shortest paths from v to w_1, w_2 and w_3 are indicated. The set W is actually a resolving set for the graph, since all vertices have unique codes. However, it is not a minimum resolving set, because $W - \{w_3\}$ is also a resolving set, which is the smallest resolving set possible.

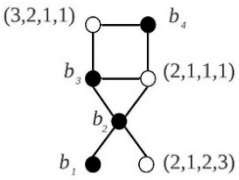

FIGURE 4. Example of an unweighted graph with a resolving vertex cover $B = \{b_1, b_2, b_3, b_4\}$. For any edge $e = uv$ in the graph, either $u \in S$ or $v \in S$, and all vertices in $V(G) - B$ have unique metric representation.

where $d(v, w_i)$ is the shortest distance from v to w_i, $1 \leq i \leq k$. W is said to be a *resolving set for* G if no two distinct vertices have the same metric representation, i.e. no two codes are the same. The objective is therefore to choose a set of vertices to form W such that each vertex in the graph has a unique code with respect to its location to W. A *minimum resolving set* of a graph G is a resolving set with the least number of elements, or in other words, the minimum amount of vertices in W for which all codes are unique.

The cardinality of a minimum resolving set is referred to as the *metric dimension* of the graph G, or dim (G). It is worth noting that a resolving set (or minimum resolving sets) is not necessarily unique, for example, any two pendant vertices (those with degree 1) in Fig. 3 could have been chosen for W with similar results.

The concept of resolving sets can be useful in finding the least amount of buses where detectors can be installed, were the objective simply to pinpoint faults occurring at buses in the grid. Since the aim of this paper is to present a scheme for fault detection and location, particularly faults occurring *within*

lines on the grid, a resolving set on its own might not necessarily be sufficient. However, when considering travelling waves that are reflected, the concept of a resolving set plays a vital role to ensure unique locations within the grid.

In order to represent physical distance in the model, we assign a weight of l_{uv} to an edge uv that has has length l_{uv}. This weighted graph is denoted by G_w. It is then possible to define a *weighted resolving set*, where the weighted metric representation of a vertex v with respect to W is defined as

$$r_w(v \mid W) = (d_w(v, w_1), d_w(v, w_2), \ldots, d_w(v, w_k)) \quad (6)$$

where $d_w(v, w_i)$ is the shortest weighted distance from v to w_i for $1 \leq i \leq k$ (note that this is not necessarily along the shortest path in the unweighted graph G). W will be weighted resolving set for G_w if $r_w(u \mid W) = r_W(v|W)$ implies that $u = v$.

B. VERTEX COVERS

A vertex cover of a graph G is a set of vertices $S = \{s_1, s_2, \ldots, s_l\}$ from $V(G)$ with the property that for any edge $e = uv$ in the graph, either u or v is in S [26]. The minimum l for which this is possible is called the vertex covering number, denoted by $\beta(G)$.

Where the (weighted) resolving sets play a role in uniquely identifying positions within the graph based on distance towards a specified set of detectors, the vertex cover literally "covers" all the edges in the graph. In other words, a travelling wave would pass through at most 1 bus before reaching the closest detector. Using a vertex cover therefore minimizes the number of possible reflected wave arrival times to consider when trying to locate the fault.

The set of solid vertices in Fig. 3 is not a vertex cover for the graph, as the edges uv, vw, xy, xw, and yz are not covered by W. The reader is referred to Fig. 4, where both a resolving set and vertex cover are presented. The minimum cardinality of a resolving vertex cover for this graph G is 4, while dim $(G) = 2$ and $\beta(G) = 3$.

C. GRAPH CONTRACTION

One important transformation that needs to occur before the detector placement algorithm can be implemented, is that of a distance-preserving graph (or vertex) contraction similar to what is found in [32]. From Section III(B), one can clearly see that if a grid contains multiple large cycles (or, more specifically, many consecutive vertices of degree 2), the vertex cover would require that every second vertex be part of the covering set. If this were to be a consideration for detector placement, it would mean that every second bus would need a detector, which is clearly impractical and wasteful of expensive resources. A graph contraction is proposed, where buses that are not ideal locations for detectors (i.e. many consecutive buses in series with no branching) are removed.

The contraction proposed here is a slight modification of the distance-preserving contraction in [32]. For a path P_n on n vertices $v_1, v_2, \ldots, v_n$ of weighted length l_w, the interior vertices $v_2, v_3, \ldots v_{n-1}$ are removed, with the contracted graph being P_2, having vertices v_1 and v_n with weighted length l_w (See Fig. 5(a)).

For a cycle C_n with vertices $v_1, v_2, \ldots, v_n$ of weighted length l, all but one of the interior vertices are removed, say $v_3, v_4, \ldots, v_{n-1}$, so that the resulting contracted graph is a triangle C_3 consisting of v_1, v_2 and v_n, of weighted length l_w (See Fig. 5(b)). With the removal of vertices $v_3, v_4, \ldots, v_{n-1}$

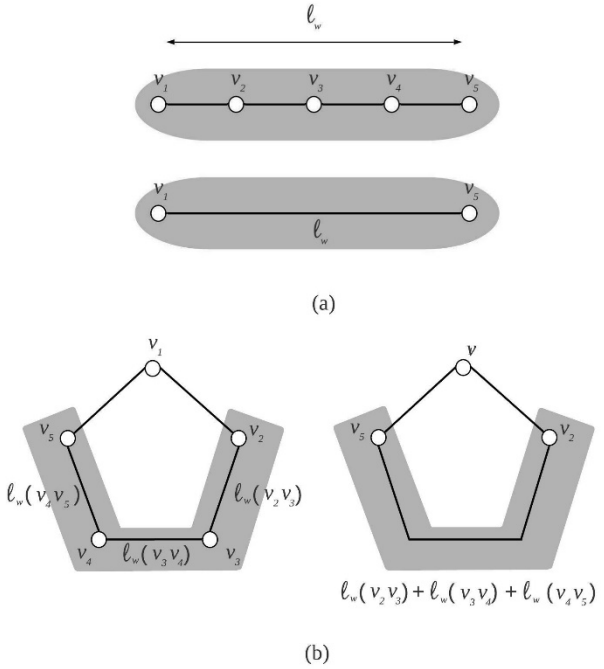

FIGURE 5. Distance-preserving graph contractions performed on (a) a path P_5 of length l_w. by removing vertices v_2,v_3 and v_4 and (b) a cycle P_5 by removing vertices v_3 and v_4, where the distance of the path $v_2v_3v_4v_5$ is preserved for the new edge v_2v_5.

the new edge v_2v_n is assigned the weighted length

$$l_w\,(v_2v_n) = \sum_{i=2}^{n-1} l_w(v_iv_{i+1}) \tag{7}$$

which is the combined weighted lengths of all edges between removed vertices and v_2 and v_n.

The method for distance-preserving graph contractions proposed here focuses on removing vertices of degree 2 and joining their incident edges. However when contracting any cycle, the smallest that the cycle can be contracted is 3 vertices. This is to avoid contracting the graph into a non-simple graph, i.e. more than one edge between vertices.

D. DETECTOR PLACEMENT

The placement algorithm in this paper is based on finding a set of vertices that is both a weighted resolving set, as well as a vertex cover. However, first a distance-preserving contraction as described in the previous section is performed on the weighted graph G_w. Two additional constraints are introduced to ensure that no location on any edge can be mistaken for another. The first is that no path between any two vertices in the detector set can have the same (weighted) distance, and the second is that all but one pendant vertex adjacent to the same vertex cannot all be outside of the detector set. In order to find the smallest set $B = \{b_1, b_2, \ldots, b_k\}$ of detectors, a detection algorithm is proposed as described in Fig. 6.

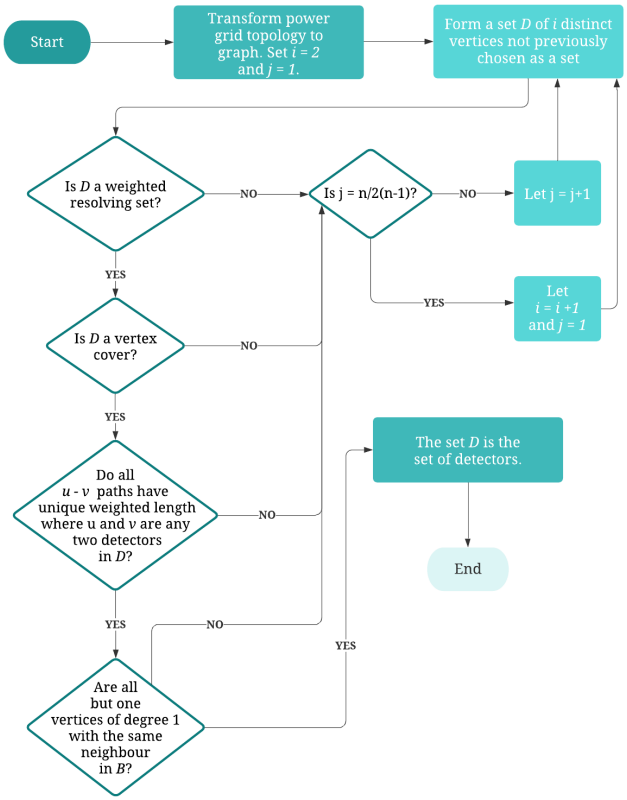

FIGURE 6. A flowchart illustrating the process of the detector placement algorithm.

IV. PROPOSED ONLINE ALGORITHM FOR FAULT LOCATION

After performing the offline operation of optimal detector placement in Section III and assuming that appropriate detectors are place at the identified nodes in the electrical network, the core of the online algorithm could be considered active.

Suppose the primary wave arrival times at the k chosen detectors are given by the vector $P = [t_{D_1}, t_{D_2}, \ldots, t_{D_k}]$ (in ms). If the two smallest values in P correspond to the primary wave arrival times at two detectors D_u and D_v, then these two detectors are closest (along the grid) to where the fault occurs.

There are a few possibilities for the fault location in terms of its position to vertices u and v in the graph. Firstly, the fault could occur on some $u - v$ path (not necessarily the shortest), and the two earliest arrival times at u and v are extracted from travelling waves that propagated from two different directions at the fault occurrence point. This first scenario is illustrated in Fig. 7, and is referred to as an internal fault. Secondly, it is possible for the two earliest travelling waves detected to have originated from the same end of the fault. This is referred to as an external fault. Here are two cases. For the first, the wave reaches one of the detectors (say u) first, and then travels towards the second detector via the shortest $u - v$ path, see Fig. 8. In the second case, the wave travels through one

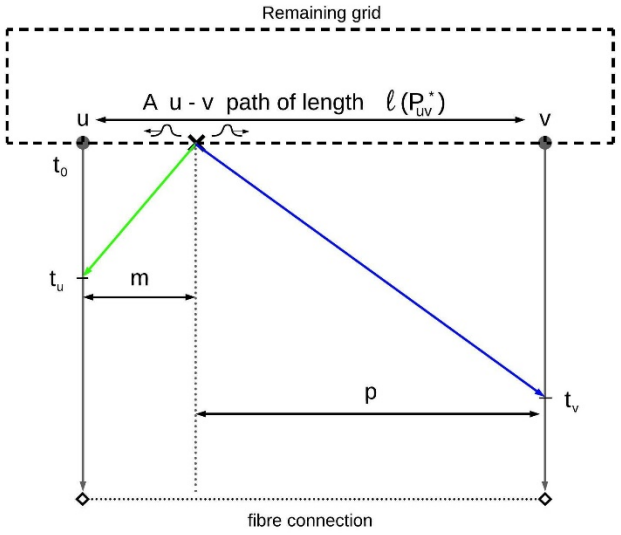

FIGURE 7. An example of an internal fault occurring along a $u-v$ path P_{uv}^* of (weighted) length $l(P_{uv}^*)$, where the primary waves reach u and v by propagating in opposite directions from the fault occurrence point. A Bewley diagram is incorporated to illustrate the timeline (using the two solid vertical axes) starting at the fault occurrence time t_0. The time t_u and t_v represents the arrival times of these primary waves at detectors u and v, respectively. The distance from the fault towards detector u is shown as m, and the distance from the fault towards detector v is shown as p.

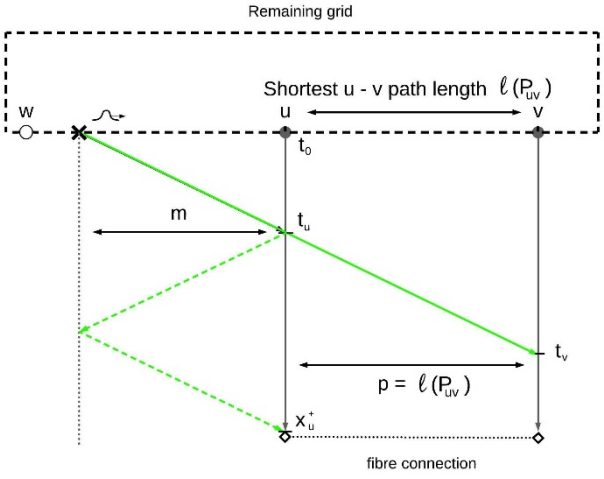

FIGURE 8. An example of an external fault, where the primary travelling wave reaches one of the detectors (say u) first, and then travels towards the second detector via the shortest $u-v$ path P_{uv} of (weighted) length $l(P_{uv})$. In this case, the earliest primary waves reach u and v by propagating in the same direction from the fault occurrence point. A Bewley diagram is incorporated to illustrate the timeline (using the two solid vertical axes) starting at the fault occurrence time t_0. The time t_u and t_v represents the arrival times of these primary waves at detectors u and v, respectively, and reflections are also indicated between detectors, the fault, and possible vertices along these paths. The distance from the fault towards detector u is shown as m, and the distance from the fault towards detector v is shown as $m+p=m+l(P_{uv})$.

or more common vertices (non-detectors) and refracts from the final common vertex in two directions towards vertices u and v, see Fig. 9.

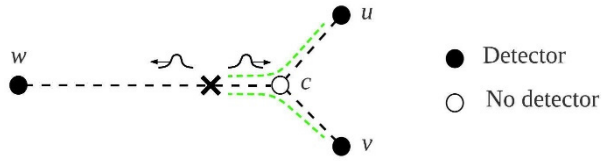

FIGURE 9. An example of an external fault, where the primary travelling wave travels along one or more common vertices like c (that are non-detectors) first, and then towards detectors u and v in opposite directions.

In the case of an internal fault occurring on a $u-v$ path P_{uv}^* of length $l\left(P_{uv}^*\right)$, the fraction $x^{uv}=\frac{m}{l(P_{uv}^*)}$ of the length of P_{uv}^* can be described by

$$x^{uv}=\frac{T_{uv}^*+(t_u-t_v)}{2T_{uv}^*}, \tag{8}$$

where T_{uv}^* is the transmission time of P_{uv}^* [30].

In the second case, a fault occurs externally and the travelling wave first reaches one of the detectors, say u and then moves along the shortest $u-v$ path towards v. As indicated in Fig. 8, The travelling wave from the fault, reflecting at u, again reflecting from the fault back to u arrives at time x_u^+ with positive polarity. This is not necessarily the secondary wave s_{D_u} that arrives at u, since the presence of possible vertices between the fault and v, or beyond the fault in the opposite direction, could result in a travelling wave that reaches u before the reflected fault wave. If one could identify x_u^+ successfully, it is possible to find the distance m from the fault to u (and then certainly the distance to v) by using the formula

$$m=\frac{\left(x_u^+-t_u\right)v}{2}, \tag{9}$$

$$x^{uw}=\frac{\left(x_u^+-t_u\right)}{2T_{uw}^*}, \tag{10}$$

where v here denotes the line speed, $x^{uw}l_{uw}^e=m$ denotes the fraction of the line from u to w corresponding to the section between the fault and u, and l_{uw}^e the length of line uw. One can easily identify the possibility of this type of external fault for two detectors u and v if $t_v-t_u=T_{uv}$. This could imply that the wave travels through detector u first, and then along the shortest $u-v$ path towards vertex v (similarly $t_u-t_v=T_{uv}$ could imply that the wave travels through detector v first, and then towards u).

In the case of Fig. 9, an external fault that results in a travelling wave moving towards the two closest detectors u and v in the same direction, there must be a final common vertex through which this wave passes, say c, before it diverges towards u and v. Necessarily, c cannot be a detector, but because the detector set must be a vertex cover for the contracted graph, the edge on which the fault occurs must lie on some $w-c$ path where w is a detector. This means the fault is external in terms of u and v, but is internal for detectors u, w and vw, and Equation (8) can be used to determine the position of the fault.

For an internal fault, only the primary wave arrival times are necessary in order to locate the fault occurrence point, which are readily available. The fault location calculated from these arrival times can be confirmed by looking for the occurrence of a specific reflected wave at the nearest detector (match). However, in order to identify an external fault's location, the method in this paper theoretically assumes that all arrival times as well as polarities at are available at all detectors. Currently, while theoretically possible, it is difficult in practice to detect reflected waves beyond a certain point, especially for power networks with many paths. Their amplitudes become weaker as they propagate through the grid, and polarity also becomes difficult to distinguish. Fault location accuracy thus diminishes when using second, third, etc. waves as opposed to primary waves with large signal-to-noise ratio. The sampling rate could play an important role here, as it ultimately determines the accuracy and the ability to detect higher order reflected waves. As detectors become more advanced, the sampling rate will increase, which opens up the possibility of detecting and subsequently finding arrival times and polarities for reflected waves more accurately [34].

The external fault location strategy presented in Section III(B) is conceptual, and depends on future advancements in sampling rates associated with detectors. Should the reader wish to apply it to an existing dataset for fault location, where reflected wave arrival times are not accurately available, it is suggested that the detection algorithm is altered by adding the requirement that the detector set has to include all pendant vertices in the graph, instead of all but one that have common neighbours. This is a small change, but one which will ensure that all faults occur internally. The amount of additional detectors will be marginally higher, but only primary wave arrival times are required. This method, using primary waves only is explained in Section III(A), and in Section III(B) the conceptual strategy for dealing with external faults is presented.

A. INTERNAL FAULTS

How would the internal faults be distinguished from the external faults? And is it possible for a fault to be external for any two detector pairs? As mentioned previously, if

$$|t_u - t_v| = T_{uv}, \tag{11}$$

then the possibility exists that the travelling wave passes through u or v first, before reaching the other. If Equation (11) does not hold for a pair of detectors u and v, the fault can be classified as internal with respect to u and v.

If it is possible to find two detectors u and v for which Equation (11) does not hold, with earliest primary arrival times from P, the array

$$T = [T^1_{uv}, T^2_{uv}, \ldots, T^r_{uv}] \tag{12}$$

represents the transmission times along each distinct $u - v$ path, and the array X is formed with r entries

$$x^{uv}_i = \frac{T^i_{uv} + (t_u - t_v)}{2T^i_{uv}} \tag{13}$$

each representing the fraction of the i-th $u - v$ path with transmission time T^i_{uv} for $1 \leq i \leq r$. These entries are therefore the fractions of the $u - v$ paths' total lengths (from the fault to u).

The fault occurs along one of these r paths, say P^i_{uv}. Thus the fault occurrence time t^i_0 [30] can be found by calculating

$$t^i_0 = \frac{t_u + t_v - T^i_{uv}}{2}. \tag{14}$$

Theoretically, then, if the fault occurs along path P^i_{uv} at time t^i_0, the reflected wave from u to the fault and back would occur at time $x^+_u = t^i_0 + 3(t_u - t^i_0)$ with positive polarity (see Fig. 7). Because of the detector placement, this timestamp will be unique, i.e. it will only occur along one particular path. It is therefore proposed that $t^i_0 + 3\left(t_u - t^i_0\right)$ is calculated for all i where $1 \leq i \leq r$ and compared to arrival times at detector u with positive polarity. If there is a time detected at u that matches $t^i_0 + 3\left(t_u - t^i_0\right)$, then the fault occurs along path P^i_{uv}, and the distance from u along this path will be

$$m_i = x^{uv}_i l\left(P^i_{uv}\right) \tag{15}$$

where x^{uv}_i is the fraction of the uv path in Equation 12, and $l(P^i_{uv})$ is the length of path P^i_{uv}.

B. EXTERNAL FAULTS

If, for a detector set $K = \{D_1, D_2, \ldots, D_k\}$, it is possible to find a detector u for which $t_{D_i} - t_u = T_{uD_i}$ for all $i \in [1, k] - u$, then the fault is external for all possible detectors, and occurs either on a pendant edge in the graph, or a leg on the graph. A leg of a graph is a path from a vertex (u in this case) that ends in a pendant vertex, where all internal vertices on the path have degree 2. This will be a special case for which Equations (9-10) will be used. In this particular application, the presence of a leg on a power grid of length more than 1 is highly unlikely, and because of the choice of detector placement it would not be unreasonable to assume that there can only be one edge along which the fault can occur, namely the only pendant edge incident with u, whose pendant vertex w does not have a detector. It then simply remains to find the distance from the fault to the closest detector.

From the primary wave array $P = [t_{D_1}, t_{D_2}, \ldots, t_{D_k}]$, detector $u = D_1$ would be the first detector reached at time $t_u = t_{D_1}$, but the reflected wave's arrival time (from u to the fault and back), say x^+_u (see Fig. 8), would not necessarily be linked to the secondary wave that arrives at u.

If the fault occurrence point is closer to u than any other vertex (except of course, w) is to u, then x^+_u is the secondary wave that arrives at u, but if it lies further from u than these vertices, the second time of arrival at u will be received from a wave reflecting not from the fault, but from one or more of these vertices, hence Equations (9-10) will give

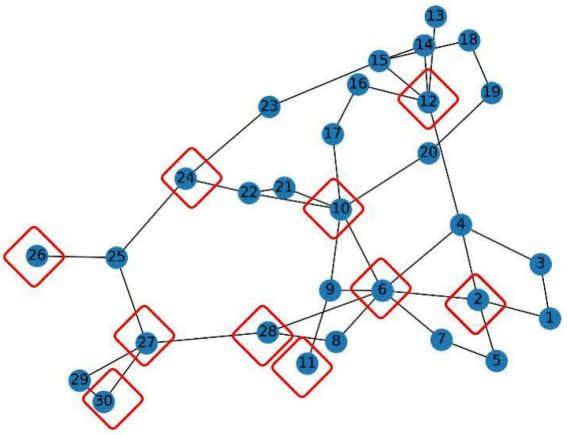

FIGURE 10. Graph representation of the IEEE 30-bus distribution system (Generated using pandapower [33]). Detectors are placed at buses 2, 6, 10, 11, 12, 24, 26, 27, 28 and 30.

inaccurate values. From the arrival times at detector u, it is impossible – at first glance – to determine which of these is the case.

Suppose, however, that it is possible to identify the reflected fault wave at time x_u^+. The distance m could be calculated easily using Equation (9). If the fault occurs along edge $e = uw$, then there would again be a wave travelling to bus u, back to the fault, and reflected back to bus u. This wave would travel a distance of $3m$, arriving at time

$$t_0 + 3\,(t_u - t_0) \tag{16}$$

where $t_0 = \frac{1}{2}\left(3t_u - x_u^+\right)$. If it were possible to retrieve several arrival times at detector u, say $U = [t_u = u_1, u_2, u_3, \ldots, u_n]$, one would be able to use Equation (9) to calculate n distances from u, one of which would be the distance to the fault. But how would one go about identifying it?

Firstly, as can be seen in Fig. 8, the reflected wave from the fault has positive polarity, and so all u_i with negative polarity can be discarded. Secondly, if some $u_i = x_u^+$, then the reflected wave (from the fault to u back to the fault, and again back to u) would have an arrival time of

$$u_j = t_0 + 3\,(t_u - t_0)\,. \tag{17}$$

for some $j = 2, 3, \ldots, n$, with positive polarity. One can therefore form a partition of U into two arrays U^+ and U^-, containing arrival times with positive and negative polarity, respectively. Then calculate and match all distances corresponding to the arrival times in U^+. If it is possible to find a $u_i \in U^+$ and $u_j \in U^+$, that satisfies Equation (16), that is, $t_j = t_0 + 3\,(t_u - t_0)$ as well as $t_0 = \frac{1}{2}\,(3t_u - u_i)$, then the distance from the fault to u will be $m_i = \frac{(u_i - u_1)v}{2}$ (from Equation (9)) from u along line uw, and the fault has been located.

V. SIMULATION RESULTS

The methodology of the optimal placement of detectors (see Section III) was applied to the graph representation of the IEEE-30 distribution system (see Fig. 10) and the optimal placement of detectors was determined to be at buses 2, 6, 10, 11, 12, 24, 26, 27, 28 and 30. In order to benchmark the proposed alternative travelling wave fault locating algorithm, the fault location generated by the online algorithm was compared to the results obtained in [30]. Table 1 shows transmission line lengths and wave-propagation time adopted from [30].

TABLE 1. Transmission line lengths and wave-propagation times for all lines of the IEEE-30 bus adopted from [30].

Line	Length (km)	Time (ms)	Line	Length (km)	Time (ms)
1-2	67	0.2246	12-13	30	0.1005
1-3	438	1.4685	12-14	365	1.2238
2-4	389	1.3042	12-15	434	1.4551
2-5	82	0.2749	12-16	158	0.5297
2-6	386	1.2942	14-15	238	0.7979
3-4	128	0.4291	15-18	59	0.1978
4-6	179	0.6001	15-23	216	0.7242
4-12	43	0.1441	16-17	248	0.8315
5-7	277	0.9287	18-19	368	1.2338
6-7	47	0.1557	19-20	299	1.0025
6-8	346	1.1601	21-22	107	0.3587
6-9	310	1.0393	22-24	248	0.8315
6-10	264	0.8851	23-24	221	0.7409
6-28	222	0.7443	24-25	384	1.2875
8-28	309	1.0360	25-26	190	0.6370
9-10	154	0.5163	25-27	374	1.2539
9-11	98	0.3285	27-28	307	1.0293
10-17	186	0.6236	27-29	381	1.2774
10-20	104	1.3487	27-30	259	0.8663
10-21	352	1.1802	29-30	178	0.5968
10-22	326	1.0930			

A. INTERNAL FAULTS

The fault from [30] on line $2-6$ with inception time of 10ms was simulated for new detector placements at buses 2, 6, 10, 11, 12, 24, 26, 27, 28 and 30. The fault occurred at a distance of 200 km along the line $2-6$ from bus 2.

EMPT was used for the simulation of the fault within the IEEE-30 bus distribution system and morphological edge detection was utilized for time stamping of primary, secondary and tertiary waves (see Table 2 and [30] with T1, T2 and T3 representing arrival times for primary, secondary and tertiary waves with polarity P1, P2 and P3 at detectors 2 and 6). Detectors 2 and 6 are the two nearest detectors to the fault, based on their primary wave arrival times being the earliest, occurring at 10.679 and 10.632, respectively.

To accurately estimate the fault location, the measured voltage signals are first converted to their modal components. The modal components are processed through the discrete wavelet transform (DWT) and the wavelet coefficients (WC) are retrieved and employed to detect the arrival times and polarity of travelling wave. Arrival time of initial traveling wave-front is captured according to modulus maximum of the wavelet transform. The WCs of traveling wave at bus 6 for

TABLE 2. Arrival times and polarity of travelling wave at detectors 2 and 6 when fault occurs 200 km away from bus 2 on line 2-6.

		D2	D6
Time	T1	10.679	10.632
	T2	11.132	10.95
	T3	11.233	11.267
Polarity	P1	-	-
	P2	+	+
	P3	+	+

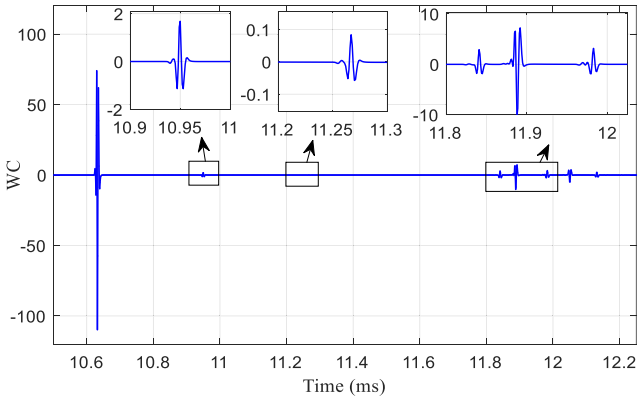

FIGURE 11. WC of the traveling wave at bus 6 for fault on the line 2-6.

TABLE 3. The 4 shortest $2-6$ (or $6-2$) paths with their lengths and transmission times.

i	Path	Length (km)	Time (ms)
1	2-6	386	1.2942
2	2-5-7-6	406	1.3593
3	2-4-6	568	1.9043
4	2-1-3-4-6	812	2.7223

fault on the line 2-6 are shown in Fig. 11. The fault occurs internally along a $6-2$ path, since $|t_2 - t_6| = 0.047 \neq T_{26} \approx 1.2942$ (Equation (11)). The 4 shortest $6-2$ (or $2-6$) paths are shown in Table 3. For each $6-2$ path, a possible fault inception time can be calculated using Equations (13) and (14).

Firstly, $x_i^{6,2}$ can be calculated for each $6-2$ path $P_{6,2}^i$ with transmission time $T_{6,2}^i$. This represents the fraction of the path corresponding to the distance from the closest detector (bus 6) to the fault using Equation (13). Each possible fault inception time t_0^i is then calculated using $x_i^{6,2}$ and Equation (14). Finally, all values of $t_0^i + 3\left(t_6 - t_0^i\right)$ are calculated, which represent the possible reflected waves with positive polarity detected at bus 6. Table 4 shows these fractions, fault inception times and possible reflected wave arrival times for the 4 shortest $6-2$ paths.

Matching these values with the arrival times at bus 6, one can see that t_0^i corresponds to the detected waves at time $t \approx 11.8792$, and so the fault occurs along the shortest $6-2$ path with transmission time $T_{6,2} \approx 1.2942$. From Table 4, the fraction of the line $6-2$ is equal to roughly 0.4818 and the distance calculated from bus 6 will

TABLE 4. The values of $x_i^{6,2}$ and t_0^i for the 4 shortest $2-6$ (or $(6-2)$ paths, calculated using Equations (13) and (14).

i	Path	$x_i^{6,2}$	t_0^i	$t_0^i + 3(t_6 - t_0^i)$
1	**2-6**	**0.4818**	**10.0084**	**11.8792**
2	2-5-7-6	0.4827	9.9759	11.9442
3	2-4-6	0.4877	9.7034	12.4892
4	2-1-3-4-6	0.4914	9.2944	13.3072

TABLE 5. Primary travelling wave arrival times at buses 2, 6, 10, 11, 12, 24, 26, 27, 28 and 30, where the fault occurs 5 km away from bus 12 on line 12-13. The nearest detector to the fault is D12.

Detectors	Arrival times (ms)	Detectors	Arrival times (ms)
D2	11.669	D24	12.962
D6	10.771	D26	14.462
D10	11.662	D27	12.557
D11	12.148	D28	11.52
D12	10.021	D30	13.432

TABLE 6. Arrival times and polarity of travelling waves at detector 12, where the fault occurs 5 km away from bus 12 on line 12-13.

		D12
Time	T1	10.021
	T2	10.055
	T3	10.089
Polarity	P1	+
	P2	+
	P3	+

be $x_1^{6,2} \times l\left(P_{6,2}^1\right) \approx 185.9748$ km, which is roughly 200.0252 km from bus 2.

B. EXTERNAL FAULTS

An external fault for the IEEE-30 bus from [30] was simulated on line $12-13$, at a distance of 5 km from bus 12 with inception time at 10ms. Primary travelling wave arrival times at detectors 2, 6, 10, 11, 12, 24, 26, 27, 28 and 30 are shown in Table 5, and arrival times at the nearest detector (bus 12) are shown in Table 6 for primary, secondary and tertiary waves with polarity P1, P2 and P3. It can be confirmed that the fault is indeed external by noting that $|t_{12} - t_v| = T_{12,v} + \epsilon$ for all detectors $v \neq 12$ and a specified error margin ϵ, thus the travelling wave passes through detector 12 before reaching any of the others.

Using Equation (9) and primary wave arrival time $t_{12} = 10.105$ along with secondary, tertiary, etc. arrival times with positive polarity (such as $T2 = 10.308$ in Table 5), a set of possible distances from bus 12 along the line $12-13$ can be derived. A set of possible fractions corresponding to the section on line $12-13$ from bus 12 to the fault can be found from Equation (10), which in turn can be used to find a set of predicted reflected travelling wave arrival times (specifically travelling waves from the fault to bus 13, and back to 12). It is possible to find these using Equation (16).

As an example $x^{12,13} = \frac{(10.055-10.021)}{2T_{12,13}} \approx 0.1692$ and $t_0 \approx 10.004$. The distance from bus 12 would be

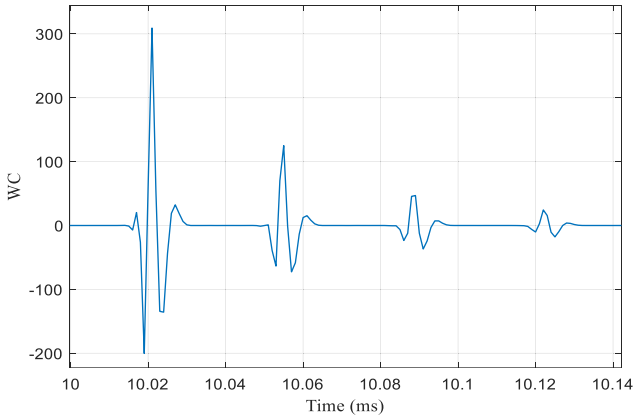

FIGURE 12. WC of the traveling wave at bus 12 for fault on the line 12-13.

approximately 5.0746 km. The expected arrival time of a reflected travelling wave would be approximately at time 10.055. Fig. 12 shows the WC of the travelling waves at bus 12, with a matching arrival time of 10.055, which can also be confirmed from Table 6 as T2. Thus the fault has been located.

As mentioned earlier, this method of identifying reflected travelling waves could possibly extend past current practical capabilities, as it is difficult to detect a great number of reflected waves and their polarities. However, should a number of possible distances be calculated from arrival times, none of which match with the data for the reflected waves, it would imply that the distance of the fault to the nearest bus u must exceed all of the distances calculated (from incorrectly assumed x_u^+). Depending on the number of reflected waves with positive polarity, one can thus use this process of elimination to determine a lower bound for the distance from the nearest bus to where the fault can occur.

VI. DISCUSSION

The error of the fault estimation where the fault occurs on the i-th $u-v$ path can be expressed as a percentage δ_{FL}^i as follows:

$$\delta_{FL}^i = \frac{\left|\left(m_A^i - m_O^i\right)\right|}{l(P_{u,v}^i)} \times 100 \tag{18}$$

where $m_A^i, m_O^i, l(P_{uv}^i)$ represent the actual distance along the i-th $u-v$ path from the fault to bus u, the calculated distance along the i-th $u-v$ path from the fault to bus u, and the length of the i-th $u-v$ path.

For the simulated internal fault on the IEEE-30 bus that occurred 200 km from bus 2 on line $2-6$, the proposed algorithm was able to identify the fault on line $2-6$ at a distance of 200.0252 km from bus 2. The percentage error of the proposed fault location scheme is therefore equal to 0.0065%, this compares well with the results of 0.0066% obtained in [30] (See Table 6 in [30] for a comparison to recent wide-area fault location methods).

For the external fault simulation along line 12-13, the actual distance from bus 12 was 5 km, and the calculated distance from bus 12 was found to be 5.0746 km. This gives a percentage error of 0.0025%, which is negligible.

VII. CONCLUSION

In this paper, a graph theory-based approach is presented as a solution for investigating an optimal and unique TWFL detection scheme for power grids containing several paths for fault travelling wave propagation. The main contributions of the paper can be summarized as follows:

1) A proposed placement strategy for detectors based on a combination of the graph theoretic concepts of vertex covers and resolving sets. The vertex cover requirement for detectors ensures that every line (or successive lines that do not branch out for the contracted graph) has a detector at one end. The requirement that the placement of detectors must also correspond to a set of vertices that are able to distinguish all other vertices in the graph based on their distances to this set ensures that the origin of any reflected travelling waves can be uniquely determined. These two concepts play a role in identifying internal or external faults and then using reflected wave arrival times to identify the unique path along which the travelling wave propagated, as well as the distance from the detector,
2) A proposed scheme for detection of both internal and external faults, based on fault wave arrival times and polarization. Based on the two earliest primary wave arrival times at detectors, the fault can be classified as internal or external and a relatively straightforward approach is shown for either case to identify the line on which the fault occurs, as well as the distance to the nearest detector,
3) Simulation results based on the IEEE-30 bus network were presented, which verified that the proposed detection scheme can accurately and uniquely determine both internal and external faults. These results were benchmarked against similar wide-area fault location methods and improvements were observed regarding the accuracy of the fault location.

This work can be expanded into several innovative and critical research themes. Propagation of measurement uncertainty through the proposed offline and online fault location scheme remains an interesting problem. Defining future meter requirements and accuracies needed to detect external faults in a network-independent fashion, will be explored in a future paper. Investigating the theoretical performance of the proposed scheme for travelling wave fault detection in LV networks and the necessities it poses, will establish future requirements for fault location in more complex networks. Also, with some networks implementing gas insulated transmission lines (GIL), an interesting avenue to explore would be the influence of mechanical and discharge faults on the performance of the proposed fault location scheme. Immediate next steps include: investigating the influence of the effects of physical behaviors of power systems on the proposed scheme, scaling to larger networks, determining

computational complexities linked to network size and topology and benchmarking the proposed scheme using a real fault.

REFERENCES

[1] M. Farmanbar, K. Parham, Ø. Arild, and C. Rong, "A widespread review of smart grids towards smart cities," *Energies*, vol. 12, no. 23, p. 4484, Nov. 2019.

[2] W. Leterme, I. Jahn, P. Ruffing, K. Sharifabadi, and D. Van Hertem, "Designing for high-voltage DC grid protection: Fault clearing strategies and protection algorithms," *IEEE Power Energy Mag.*, vol. 17, no. 3, pp. 73–81, May 2019.

[3] M. Kuzlu, M. Pipattanasompom, and S. Rahman, "A comprehensive review of smart grid related standards and protocols," in *Proc. 5th Int. Istanbul Smart Grid Cities Congr. Fair (ICSG)*, Istanbul, Turkey, Apr. 2017, pp. 12–16, doi: 10.1109/SGCF.2017.7947600.

[4] K. Dehghanpour, C. Colson, and H. Nehrir, "A survey on smart agent-based microgrids for resilient/self-healing grids," *Energies*, vol. 10, no. 5, p. 620, May 2017.

[5] M. Ul Mehmood, A. Ulasyar, A. Khattak, K. Imran, H. S. Zad, and S. Nisar, "Cloud based IoT solution for fault detection and localization in power distribution systems," *Energies*, vol. 13, no. 11, p. 2686, May 2020.

[6] N. Ayer and R. Gokaraju, "Online application of local OOS protection and graph theory for controlled islanding," *IEEE Trans. Smart Grid*, vol. 11, no. 3, pp. 1822–1832, May 2020, doi: 10.1109/TSG.2019.2943525.

[7] J. Beyza, J. M. Yusta, G. J. Correa, and H. F. Ruiz, "Vulnerability assessment of a large electrical grid by new graph theory approach," *IEEE Latin Amer. Trans.*, vol. 16, no. 2, pp. 527–535, Feb. 2018, doi: 10.1109/TLA.2018.8327409.

[8] L. Wang, H. Liu, L. Dai, and Y. Liu, "Novel method for identifying fault location of mixed lines," *Energies*, vol. 11, no. 6, p. 1529, Jun. 2018.

[9] E. O. Schweitzer, A. Guzman, M. V. Mynam, V. Skendzic, B. Kasztenny, and S. Marx, "Locating faults by the traveling waves they launch," in *Proc. 67th Annu. Conf. Protective Relay Eng.*, College Station, TX, USA, Mar. 2014, pp. 95–110, doi: 10.1109/CPRE.2014.6798997.

[10] G. Krzysztof, R. Kowalik, D. D. Rasolomampionona, and S. Anwar, "Traveling wave fault location in power transmission systems: An overview," *J. Electr. Syst.*, vol. 7, no. 3, pp. 287–296, 2011.

[11] X. Xue, M. Cheng, T. Hou, G. Wang, N. Peng, and R. Liang, "Accurate location of faults in transmission lines by compensating for the electrical distance," *Energies*, vol. 13, no. 3, p. 767, Feb. 2020.

[12] W. Tao, M. Ma, C. Fang, W. Xie, M. Ding, D. Xu, and Y. Shi, "Design and application of a distribution network phasor data concentrator," *Appl. Sci.*, vol. 10, no. 8, p. 2942, Apr. 2020.

[13] S. L. Zimath, M. A. F. Ramos, and J. E. S. Filho, "Comparison of impedance and travelling wave fault location using real faults," in *IEEE PES T&D*, New Orleans, LA, USA, Apr. 2010, pp. 1–5, doi: 10.1109/TDC.2010.5484310.

[14] R. Dashti, S. Salehizadeh, H. Shaker, and M. Tahavori, "Fault location in double circuit medium power distribution networks using an impedance-based method," *Appl. Sci.*, vol. 8, no. 7, p. 1034, Jun. 2018.

[15] S. Jamali, A. Bahmanyar, and S. Ranjbar, "Hybrid classifier for fault location in active distribution networks," *Protection Control Modern Power Syst.*, vol. 5, no. 1, pp. 1–9, Dec. 2020.

[16] M. Shafiullah and M. A. Abido, "S-transform based FFNN approach for distribution grids fault detection and classification," *IEEE Access*, vol. 6, pp. 8080–8088, 2018, doi: 10.1109/ACCESS.2018.2809045.

[17] M. Shafiullah, M. Ijaz, M. A. Abido, and Z. Al-Hamouz, "Optimized support vector machine & wavelet transform for distribution grid fault location," in *Proc. 11th IEEE Int. Conf. Compat., Power Electron. Power Eng. (CPE-POWERENG)*, Cadiz, 2017, pp. 77–82, doi: 10.1109/CPE.2017.7915148.

[18] M. Shafiullah, M. Abido, and Z. Al-Hamouz, "Wavelet-based extreme learning machine for distribution grid fault location," *IET Generat., Transmiss. Distrib.*, vol. 11, no. 11, pp. 4256–4263, Nov. 2017, doi: 10.1049/iet-gtd.2017.0656.

[19] M. Kezunovic, "Smart fault location for smart grids," *IEEE Trans. Smart Grid*, vol. 2, no. 1, pp. 11–22, Mar. 2011, doi: 10.1109/TSG.2011.2118774.

[20] T. L. Baldwin, L. Mili, M. B. Boisen, Jr., and R. Adapa, "Power system observability with minimal phasor measurement placement," *IEEE Trans. Power Syst.*, vol. 8, no. 2, pp. 707–715, May 1993, doi: 10.1109/59.260810.

[21] V. H. Quintana, A. Simoes-Costa, and A. Mandel, "Power system topological observability using a direct graph-theoretic approach," *IEEE Trans. Power App. Syst.*, vol. PAS-101, no. 3, pp. 617–626, Mar. 1982.

[22] G. Chartrand, L. Eroh, M. A. Johnson, and O. R. Oellermann, "Resolvability in graphs and the metric dimension of a graph," *Discrete Appl. Math.*, vol. 105, pp. 99–113, Oct. 2000.

[23] S. Khuller, B. Raghavachari, and A. Rosenfeld, "Landmarks in graphs," *Disc. Appl. Math*, vol. 70, pp. 217–229, Oct. 1996.

[24] P. J. Slater, "Leaves of trees," *Congr. Numer*, vol. 14, pp. 549–559, Feb. 1975.

[25] F. Harary and R. A. Melter, "On the metric dimension of a graph," *Ars Combin*, vol. 2, pp. 191–195, 1976.

[26] G. Chartrand, L. Lesniak, and P. Zhang, *Graphs and Digraphs*. Boca Raton, FL, USA: CRC Press, 2016.

[27] Y. Chen, D. Liu and B. Xu, and Bingyin, "Wide-area traveling wave fault location system based on IEC61850," *IEEE Trans. Smart Grid*, vol. 4, no. 2, pp. 1207–1215, Dec. 2013, doi: 10.1109/TSG.2012.2233767.

[28] M. Shafiullah and M. A. Abido, "A review on distribution grid fault location techniques," *Electr. Power Compon. Syst.*, vol. 45, no. 8, pp. 807–824, 2016.

[29] L. C. Andrade and T. Ponce de Leao, "Travelling wave based fault location analysis for transmission lines," in *Proc. EPJ Web Conf.*, vol. 33, Oct. 2012, p. 04005.

[30] M. Salehi, A. A. M. Birjandi, and X. Dong, "Determining minimum number and placement of fault detectors in transmission network for fault location observability," *Int. J. Electr. Power Energy Syst.*, vol. 124, Jan. 2021, Art. no. 106386, doi: 10.1016/j.ijepes.2020.106386.

[31] J.-W. Lee, W.-K. Kim, J. Han, W.-H. Jang, and C.-H. Kim, "Fault area estimation using traveling wave for wide area protection," *J. Modern Power Syst. Clean Energy*, vol. 4, no. 3, pp. 478–486, Jul. 2016.

[32] A. Bernstein, K. Däubel, Y. Disser, M. Klimm, T. Mütze, and F. Smolny, "Distance-preserving graph contractions," *SIAM J. Discrete Math.*, vol. 33, no. 3, pp. 1607–1636, Jan. 2019.

[33] L. Thurner, A. Scheidler, and F. Schäfer, "Pandapower—An open-source Python tool for convenient modeling, analysis, and optimization of electric power systems," *IEEE Trans. Power Syst.*, vol. 33, no. 6, pp. 6510–6521, Nov. 2018.

[34] F. B. Costa, F. V. Lopes, K. M. Silva, K. M. C. Dantas, R. L. S. França, M. M. Leal, and R. L. A. Ribeiro, "Mathematical development of the sampling frequency effects for improving the two-terminal traveling wave-based fault location," *Int. J. Elect. Power Energy Syst.*, vol. 115, Feb. 2019, Art. no. 105502, doi: 10.1016/j.ijepes.2019.105502.

ELIZABETH C. M. MARITZ received the master's and Ph.D. degrees in graph theory from the University of the Free State, South Africa, in 2014 and 2017, respectively.

She has been a Lecturer in mathematics at the University of the Free State, since 2011. Her research interests include additive and hereditary properties of graphs, generalized colorings of graphs, and various other graph parameters.

JACQUES M. MARITZ received the master's degree in physics and the Ph.D. degree in astrophysics from the University of the Free State, South Africa, in 2014 and 2017, respectively.

He has been a Lecturer in engineering sciences at the University of the Free State, since 2017. His research interests include physics, astrophysics, energy modeling, energy analytics, energy AI, and power systems.

MOSLEM SALEHI received the master's degree in electrical engineering from Shahid Rajaee Teacher Training University, Iran, in 2011, and the Ph.D. degree in electrical engineering from Lorestan University, Iran, in 2018.

He has been a Lecturer in electrical engineering at Technical and Vocational University (TVU), since 2019. His research interests include power system protection, and fault location and detection in power systems.